Formulation and application of rate-independent stress update algorithm of hydrostatic pressure: elastoplastic yielding in composite

Hanfeng Zhai

Department of Mechanics,
School of Mechanics and Engineering Science,
Shanghai University

June 20, 2020

Plasticity Theory

Formulation and application of rate-independent stress update algorithm of hydrostatic pressure: elastoplastic yielding in composite

Abstract

The stress update algorithm is widely adopted in the analysis of the plastic mechanism of materials. The Drucker-Prager criterion is a yield function dependent on both hydrostatic pressure and deviatoric stress. Applied with the Drucker-Prager criterion, here, we develop a stress update algorithm depicting such a process by adopting the post-yield behavior given by An. The fiber-reinforced composite is widely applied in manufacturing nowadays. The plastic effect of the matrix to the composite under tensile loading is investigated in the article, for which the Drucker-Prager criterion is adopted to delineate the mechanical behavior of the matrix. A matrix deflection mechanical effect is also taken into consideration by studying the stress-strain distribution variances. The results show that the stress is centrally concentrated while growing evenly distributed and concentrated on the fiber's 1-directional edge with the ongoing load. The strain also exhibits similar distribution at the beginning albeit concentrated at the fiber's tangential surface with the loading. With the deflection of the matrix, the 2-directional stress exhibits higher values in the local deflection region, indicating a higher possibility of the local failure in the composite. Also, the local deflection does not influence the plastic strain distribution.

Keywords: plasticity; stress update algorithm; Drucker-Prager criterion; composite materials; fiber-reinforced composite

Introduction

Plasticity is a general nature of materials. To depict such nature, one applies a model described by a constitutive equation which can be delineated by the stress algorithm [1]. The stress update algorithm could be applied to different materials, with regards to the evolution of the internal variables and the determination of the yield function ([2], [3], [4]). The rate-independent isotropic hardening plasticity is described by details such that a parametric form function k is applied to depict the update algorithm, which can be distinguished as swift, voce and swift-voce [5]. Based on such, an example of a uniaxial tensile loading acting on a cubic is presented to illustrate the application of stress-update algorithm [6] and a finite difference method in which a to homogenous anisotropic hardening model used is given as illustrating the yielding process [7]. An elastoplastic model calculated by stress update is applied to the mechanical calculation of clay [8].

The stress update algorithm could be used for the estimation of materials mechanical properties. An *et al.* presented works using the plasticity theory to depict the mechanical properties of biomaterials ([9], [10], [11], [12], [13]). Among many yield functions, with consideration of the hydrostatic pressure, the Drucker-Prager criterion could be representative. Plus, such yield function could also be applied for the explanation of the mechanisms of dentin fracture properties ([12], [13]). The mathematical basis for such a model is elucidated [14]. Furthermore, the depiction of the stress update algorithm could be applied by MATLAB code ([15], [16]).

The composite is widely adopted for manufacturing due to its spectacular mechanical properties. Also, the composite materials exhibit special elastic-plastic response with microscopic structures [17]. To delineate such, the strength of the steel-concrete composite is calculated showing plastic stress distribution method can yield significantly unconservative strength predictions, especially for encased composite members with high steel yield strengths and high steel ratios [18]. The mechanism of the particulate composite is elucidated through numerical finite element method, in which different modelling is adopted [19]. Similarly, the hierarchical structured composite's mechanical behavior is tested through different loading simulations, indicating temperature has the significant effects on the performances of 3D braided composites [20]. The rate-dependent plastic yielding of fiber-reinforced composite has also been studied by many scholars with regards to the mesoscale modelling [21], which is concentrated and studied in this paper.

Method

Analytical Solution

The strain is split into an elastic and a plastic part

$$\boldsymbol{\varepsilon} = \boldsymbol{\varepsilon}^e + \boldsymbol{\varepsilon}^p \tag{1}$$

i.e. the elastic strain is

$$\boldsymbol{\varepsilon}^e = \boldsymbol{\varepsilon} - \boldsymbol{\varepsilon}^p \tag{2}$$

Therefore, the constitutive equation for stress

$$\boldsymbol{\sigma} = \boldsymbol{C}: (\boldsymbol{\varepsilon} - \boldsymbol{\varepsilon}^p) \tag{3}$$

Where $\boldsymbol{C}$ is the fourth-order isotropic stiffness tensor taking the form

$$\boldsymbol{C} = 2G\mathbf{11} + \left(K - \frac{2}{3}G\right)\mathbf{1}\otimes\mathbf{1} \tag{4}$$

The yield function is given by Drucker-Prager criterion:

$$f(\boldsymbol{\sigma}, c) = \sqrt{\frac{3}{2}s_{ij}s_{ij}} + \frac{1}{3}\sigma_{kk}tan\beta - c \tag{5}$$

In which c denotes the cohesion force under uniaxial compression:

$$c = (1 + tan\beta)\sigma_y \tag{6}$$

Where σ_y is the uniaxial tensile yield stress. Based on the previous study of the constitutive model of cordial bone conducted by An [10], a power law strain hardening is employed to characterize the post-yield behavior

$$\sigma_y = \sigma_0\left(1 + \frac{\varepsilon^p}{\varepsilon^0}\right)^n \tag{7}$$

In the study, to simplify the reasoning, the strain hardening exponent: $n = 1$.

Where J_1 and J_2 yield surface at

$$f(\boldsymbol{\sigma}, c) = \sqrt{\frac{3}{2}}\|\boldsymbol{s}\| + tan\beta\|p\| - c = 0 \tag{8}$$

Consider the case where the yield function defines plastic potential, the flow rule of rate-independent plasticity is given by:

$$\dot{\boldsymbol{\varepsilon}}^p = \dot{\lambda}h_{ij} = \dot{\lambda}\frac{\partial f}{\partial \boldsymbol{\sigma}} = \dot{\lambda}\hat{\boldsymbol{n}} \tag{9}$$

Where $\dot{\boldsymbol{\varepsilon}}^p$ is plastic strain, $\dot{\lambda}$ is an indeterminate is an indeterminate positive quantity when $f = 0$ and $\left(\frac{\partial f}{\partial \boldsymbol{\sigma}}\right)\dot{\boldsymbol{\sigma}} = 0$, and is zero otherwise.

In either case, $\dot{\lambda}$ and f can easily be seen to obey the Kuhn–Tucker conditions of optimization theory. Thus, the loading/unloading condition is:

$$\dot{\lambda}f = 0, \quad \dot{\lambda} \geq 0, \quad f \leq 0 \tag{10}$$

In which the flow vector $\hat{\boldsymbol{n}}$ is given by

$$\hat{\boldsymbol{n}} = \frac{\partial f}{\partial \sigma_{kl}} = \frac{\partial \sqrt{\frac{3}{2} s_{ij} s_{ij}}}{\partial \sigma_{kl}} + \frac{\partial \frac{1}{3} \sigma_m tan\beta}{\partial \sigma_{kl}} - \frac{\partial c}{\partial \sigma_{kl}} \tag{11}$$

$$\hat{\boldsymbol{n}} = \frac{\partial \sqrt{3J_2}}{\partial J_2} \frac{\partial J_2}{\partial \sigma_{kl}} + \frac{tan\beta}{3} \frac{\partial \sigma_m}{\partial \sigma_{kl}} \tag{12}$$

$$\hat{\boldsymbol{n}} = \frac{\sqrt{3}}{2} J_2{}^{-\frac{1}{2}} s_{kl} + \frac{tan\beta}{3} \delta_{kl} \tag{13}$$

$$\hat{\boldsymbol{n}} = \frac{\sqrt{6}}{4} \frac{\boldsymbol{s}}{\|\boldsymbol{s}\|} + \frac{tan\beta}{3} \mathbf{1} \tag{14}$$

Where the flow vector could be divided into

$$\hat{\boldsymbol{n}}^{\boldsymbol{s}} = \frac{\sqrt{6}}{4} \frac{\boldsymbol{s}}{\|\boldsymbol{s}\|}, \qquad \hat{\boldsymbol{n}}^{p} = \frac{tan\beta}{3} \mathbf{1} \tag{15}$$

Thence, the form of consistency can be written as

$$\dot{f}(\boldsymbol{\sigma}, c) = \hat{\boldsymbol{n}} : \left(\sqrt{\frac{3}{2}} \dot{\boldsymbol{s}} + \dot{p} tan\beta \right) - \dot{c} \tag{16}$$

In which

$$\dot{\boldsymbol{s}} = 2\mu \dot{\boldsymbol{e}}, \qquad \dot{p} = K \dot{\varepsilon}_V, \qquad \dot{\boldsymbol{c}} = (1 + tan\beta)\sigma_0 \left(1 + \frac{\dot{\boldsymbol{\varepsilon}}^p}{\varepsilon^0} \right) \tag{17}$$

Thenceforth, the consistency condition takes the form

$$\dot{f} = \frac{\partial f}{\partial \boldsymbol{\sigma}} : \dot{\boldsymbol{\sigma}} - (1 + tan\beta)\sigma_0 \left(1 + \frac{\dot{\boldsymbol{\varepsilon}}^p}{\varepsilon^0} \right) \tag{18}$$

Which can be reduced into:

$$\dot{f} = \frac{\partial f}{\partial \boldsymbol{\sigma}} : \dot{\boldsymbol{\sigma}} - (1 + tan\beta)\sigma_0 \left(1 + \frac{\dot{\lambda} \hat{\boldsymbol{n}}}{\varepsilon^0} \right) \tag{19}$$

Given that

$$\hat{\boldsymbol{n}} : \dot{\boldsymbol{\sigma}} = \hat{\boldsymbol{n}} : \dot{\boldsymbol{s}} + \hat{\boldsymbol{n}} : \dot{p} \tag{20}$$

The equation can be decomposed into

$$\dot{f} = \frac{\partial f}{\partial \boldsymbol{s}} : \dot{\boldsymbol{s}} + \frac{\partial f}{\partial p} : \dot{p} \mathbf{1} - (1 + tan\beta)\sigma_0 \left(1 + \frac{\dot{\lambda} \hat{\boldsymbol{n}}}{\varepsilon^0} \right) \tag{21}$$

In which

$$\frac{\partial f}{\partial \boldsymbol{\sigma}} : \dot{\boldsymbol{\sigma}} = \frac{\partial f}{\partial \boldsymbol{s}} : \dot{\boldsymbol{s}} + \frac{\partial f}{\partial p} : \dot{p}\mathbf{1} = 2\mu\left(\hat{\boldsymbol{n}} : \dot{\boldsymbol{e}} - \dot{\lambda}\right) + E\left(\hat{\boldsymbol{n}} : \dot{\varepsilon}_V - \dot{\lambda}\right) \quad (22)$$

Hence, substituting Equation 21 into Equation 20 one deduce

$$\dot{\lambda} = \frac{\hat{\boldsymbol{n}} : (2\mu\dot{\boldsymbol{e}} + K\dot{\varepsilon}_V) - \sigma_0(1 + tan\beta)}{\sigma_0(1 + tan\beta)\left(1 + \frac{\hat{\boldsymbol{n}}}{\varepsilon^0}\right) + 2\mu + E} \quad (23)$$

Numerical solution

The first step in the numerical integration is to write the stress tensor in the predictor-corrector format,

$$\boldsymbol{\sigma}_{n+1} = \boldsymbol{\sigma}^{tr}_{n+1} - \boldsymbol{C}^e : \Delta\boldsymbol{\varepsilon}, \quad \boldsymbol{\sigma}^{tr}_{n+1} = \boldsymbol{\sigma}_{n+1} + \boldsymbol{C}^e : \Delta\boldsymbol{\varepsilon} \quad (24)$$

Using the backward implicit scheme for integrating the incremental plastic flow, one could discern:

$$\Delta\boldsymbol{\varepsilon}^p = \int_{t_n}^{t_{n+1}} \dot{\lambda}\,\hat{\boldsymbol{n}}dt \approx \Delta\lambda\hat{\boldsymbol{n}}_{n+1} \quad (25)$$

$$\hat{\boldsymbol{n}}_{n+1} = \frac{\sqrt{6}}{4}\frac{\boldsymbol{s}_{n+1}}{\|\boldsymbol{s}_{n+1}\|} + \frac{tan\beta}{3}\mathbf{1}_{n+1} \quad (26)$$

$$\Delta\lambda = \frac{a - c_n}{\sigma_0(1 + tan\beta)\left(1 + \frac{\hat{\boldsymbol{n}}_{n+1}}{\varepsilon^0}\right) + 2\mu + E} \quad (27)$$

Where $\Delta\lambda$ is the discrete plastic multiplier.

The cohesion is updated as

$$c_{n+1} = c_n + (1 + tan\beta)\sigma_0\left(1 + \frac{\varepsilon^p}{\varepsilon^0}\right) \quad (28)$$

For rate-independent plastic materials, the discrete consistency equation can be written as:

$$f_{n+1} = \sqrt{\frac{3}{2}}\|\boldsymbol{s}_{n+1}\| + p_{n+1}tan\beta - c = 0 \quad (29)$$

We take the trace of both sides of the discrete constitutive equation

$$tr(\boldsymbol{\sigma}_{n+1}) = tr(\boldsymbol{\sigma}^{tr}_{n+1}) \Rightarrow p_{n+1} = p^{tr}_{n+1} \quad (30)$$

Where $p = tr\frac{\boldsymbol{\sigma}}{3}$ is the mean normal stress.

For isotropic linearly elastic material, the elastic constitutive equations are

$$\boldsymbol{s} = 2\mu\boldsymbol{e}, \qquad p = K\varepsilon_V \tag{31}$$

Where K and μ are the elastic bulk and shear moduli, respectively.

Now, split the strain into two parts and consider each:

$$\boldsymbol{e} = \frac{\sqrt{6}}{4}\frac{\boldsymbol{s}_{n+1}}{\|\boldsymbol{s}_{n+1}\|}, \qquad \varepsilon_V = \frac{tan\beta}{3}\mathbf{1}_{n+1} \tag{32}$$

Therefore, the form of the deviatoric and mean stress is given by

$$\boldsymbol{s}_{n+1} = \boldsymbol{s}^{tr}_{n+1} - 2\mu\Delta\lambda\left(\frac{\sqrt{6}}{4}\frac{\boldsymbol{s}_{n+1}}{\|\boldsymbol{s}_{n+1}\|}\right), \qquad p_{n+1} = p^{tr}_{n+1} - K\Delta\lambda\left(\frac{tan\beta}{3}\mathbf{1}_{n+1}\right) \tag{33}$$

Therefore,

$$\hat{\boldsymbol{n}}_{n+1} = \hat{\boldsymbol{n}}^{\boldsymbol{s}}{}_{n+1} + \hat{\boldsymbol{n}}^{p}{}_{n+1} \tag{34}$$

In which

$$\hat{\boldsymbol{n}}^{\boldsymbol{s}}{}_{n+1} = \sqrt{\frac{3}{2}}\frac{\boldsymbol{s}^{tr}_{n+1}}{a}, \qquad \hat{\boldsymbol{n}}^{p}{}_{n+1} = \frac{tan\beta\mathbf{1}_{n+1}}{3a} \tag{35}$$

Step 1. Compute $\boldsymbol{\sigma}^{tr}_{n+1} = \boldsymbol{\sigma}_n + \boldsymbol{c}^e : \Delta\boldsymbol{\varepsilon}$,

$p_{n+1} = \frac{1}{3}tr(\boldsymbol{\sigma}^{tr}_{n+1})$, $\boldsymbol{s}^{tr}_{n+1} = \boldsymbol{\sigma}^{tr}_{n+1} - p_{n+1}\mathbf{1}$

Step 2. Check $a = \left\|\sqrt{\frac{3}{2}}\boldsymbol{s}^{tr}_{n+1} + tan\beta p^{tr}_{n+1}\right\| > c$?

No, set $\boldsymbol{\sigma}_{n+1} = \boldsymbol{\sigma}^{tr}_{n+1}$ and exit.

Step 3. Yes, set $\hat{\boldsymbol{n}}^{\boldsymbol{s}}{}_{n+1} = \sqrt{\frac{3}{2}}\frac{\boldsymbol{s}^{tr}_{n+1}}{a}$, $\hat{\boldsymbol{n}}^{p}{}_{n+1} = \frac{tan\beta\mathbf{1}_{n+1}}{3a}$, $\hat{\boldsymbol{n}}_{n+1} = \hat{\boldsymbol{n}}^{p}{}_{n+1} + \hat{\boldsymbol{n}}^{\boldsymbol{s}}{}_{n+1}$

$$\Delta\lambda = \frac{a - c_n}{\sigma_0(1 + tan\beta)\left(1 + \frac{\hat{\boldsymbol{n}}_{n+1}}{\varepsilon^0}\right) + 2\mu + E}$$

$\boldsymbol{\sigma}_{n+1} = \boldsymbol{\sigma}^{tr}_{n+1} - 2\mu\Delta\lambda\hat{\boldsymbol{n}}_{n+1} - E\Delta\lambda\hat{\boldsymbol{n}}_{n+1}$

$c_{n+1} = c_n + (1 + tan\beta)\sigma_0\left(1 + \frac{\varepsilon^p}{\varepsilon^0}\right)$ and exit

Box. 1 Radial return algorithm for stress update with Drucker-Prager criterion.

Problem Formulation

As mentioned in the preceding chapter the composite is now more applicated in manufacturing and engineering design more than ever ([18], [19], [20], [21]). For what is more, the plastic deformation and its compact is of great importance in the study of composite [21]. Hence, an application of the Drucker-Prager criterion is carried out to study the plastic deformation's impact of the matrix in fiber reinforced composite.

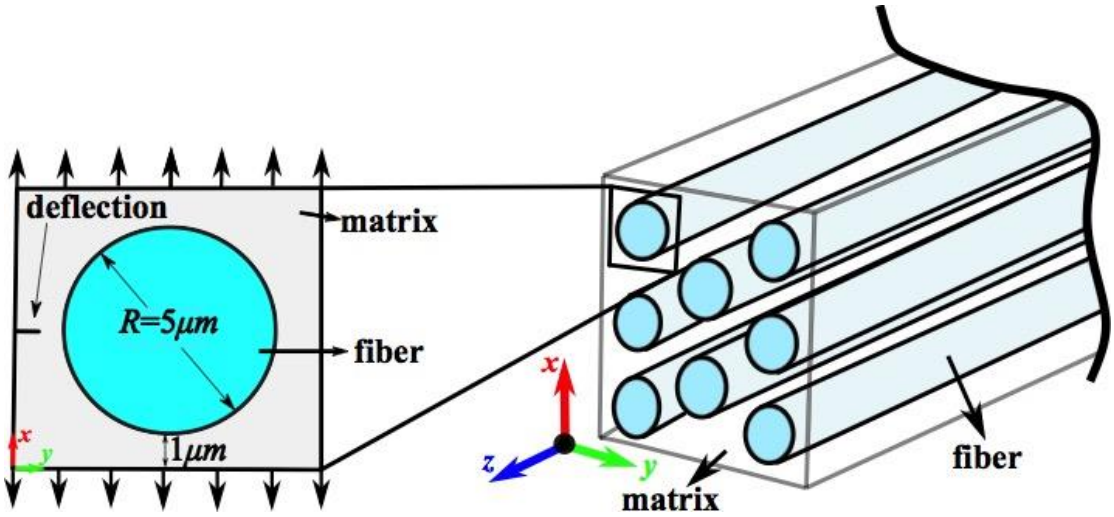

Fig. 1 Schematic illustration of the fiber reinforced composite, in which the zoomed view in the left is a "unit cell model" representative for the structure.

To study such effect, we carried out simulations applied with the Drucker-Prager criterion on the fiber-reinforced composite. The fiber-reinforced composite consists of fiber and matrix (usually consists of resin), which can be modelled as a unit cell model as shown in Figure 1. The study mainly focuses on the tensile plastic effect on the fiber-reinforced composite. For what is more, during the designing and manufacturing process, hardly prevented that deflection occurs on the composite, which usually exhibits as small fracture or cracks on the matrix as shown in Figure 1.

Such effect is also taken into consideration in the modelling that compared and discussed in the following chapter. Simultaneously, the deflection is not propagated as the ongoing loading. Here, we only consider its impact on stress-strain distribution.

Material	Elastic Modulus	Poisson's Ratio
Fiber	1GPa	0.3
Matrix	1MPa	0.3

Tab. 1 The elastic mechanical parameters for both the fiber and matrix.

The elastic mechanical parameters carried out for simulation is shown as in Table 1, in which the fiber is taken as a perfectly elastic material with high stiffness. The matrix is considered as a plastic material applied with the Drucker-Prager yield function, where the coefficients for the yield criterion is shown as in Table 2.

Yield Stress	Angle of Friction	Angle of Dilation	Flow Stress Ratio
100MPa	36	36	0.9

Tab. 2 Parameters for matrix applied for the Drucker-Prager criterion in the simulation.

Results and Discussion

Undergoing the 2-directional tensile loading, the stress σ_{22} distribution is shown as in Figure 2, in which the developing of stress distribution with loading time is presented from (a) to (f). From Figure 2 one could discern that the stress is highly concentrated in the central axis from the beginning phase. As the loading keeps, the stress is distributed evenly on both the matrix and fiber, comparatively. Howbeit the stress is highly concentrated on the 1-directional edge of the fiber and relatively low of the edge contacted matrix, which is not exhibited as the beginning stage. Also, the deformation changes from a smooth to an edged outline with the ongoing load.

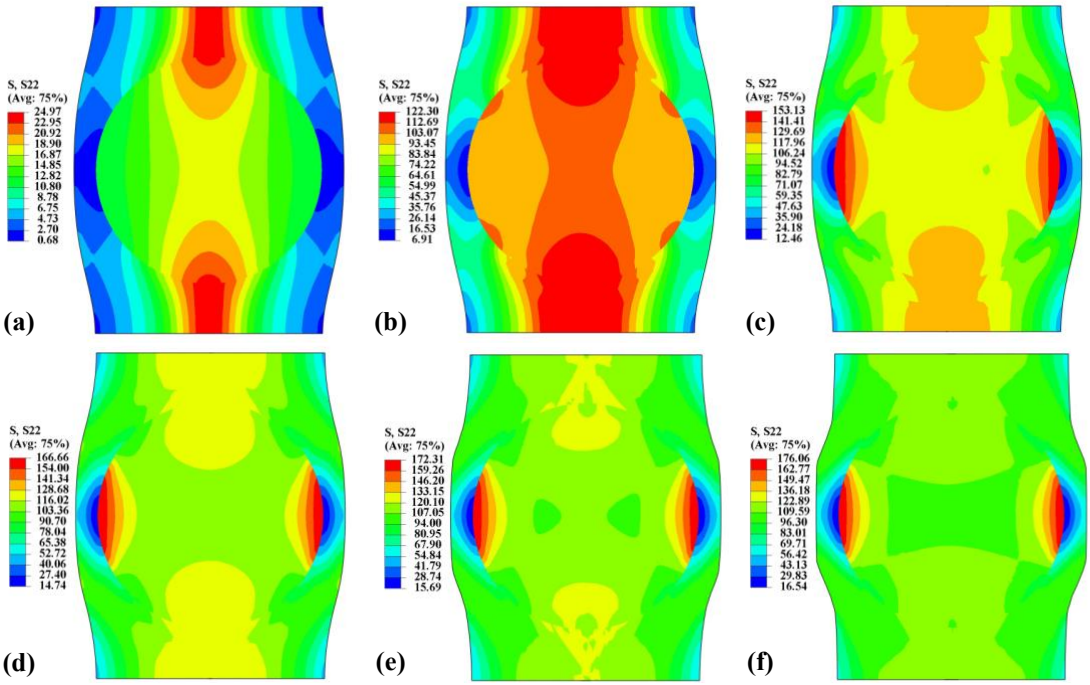

Fig. 2 The 2-directional stress distribution on the composite developing in time from (a) to (f).

The 2-directional strain distribution is also presented as in Figure 3. From the strain development, one could discern the strain concentrated on the shear surface along the fiber edge developing with time from (d) to (f).

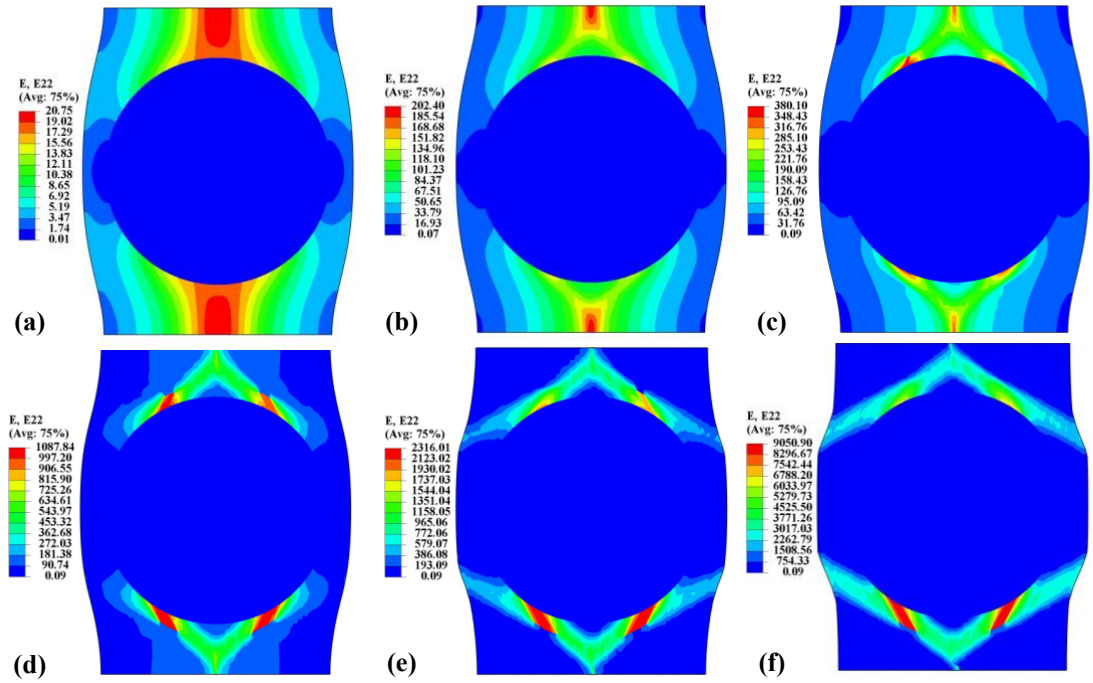

Fig. 3 The 2-directional strain distribution on the composites developing in time from (a) to (f).

Plus, at the beginning stage, the strain also exhibits similar distribution as the stress, where ε_{22} is highly concentrated along the central axis. With the ongoing load, the plastic strain concentering tangential with the fiber circular edge as shown in Figure 3(f).

Here, as mentioned in the last chapter, we elicit a deflection on the matrix of composite to investigate its effect. The 2-directional stress distribution development is shown as in Figure 4 from (b) to (f), which exhibits similar trends as in Figure 2. The zoomed view of the deflection development is shown in Figure 4(a).

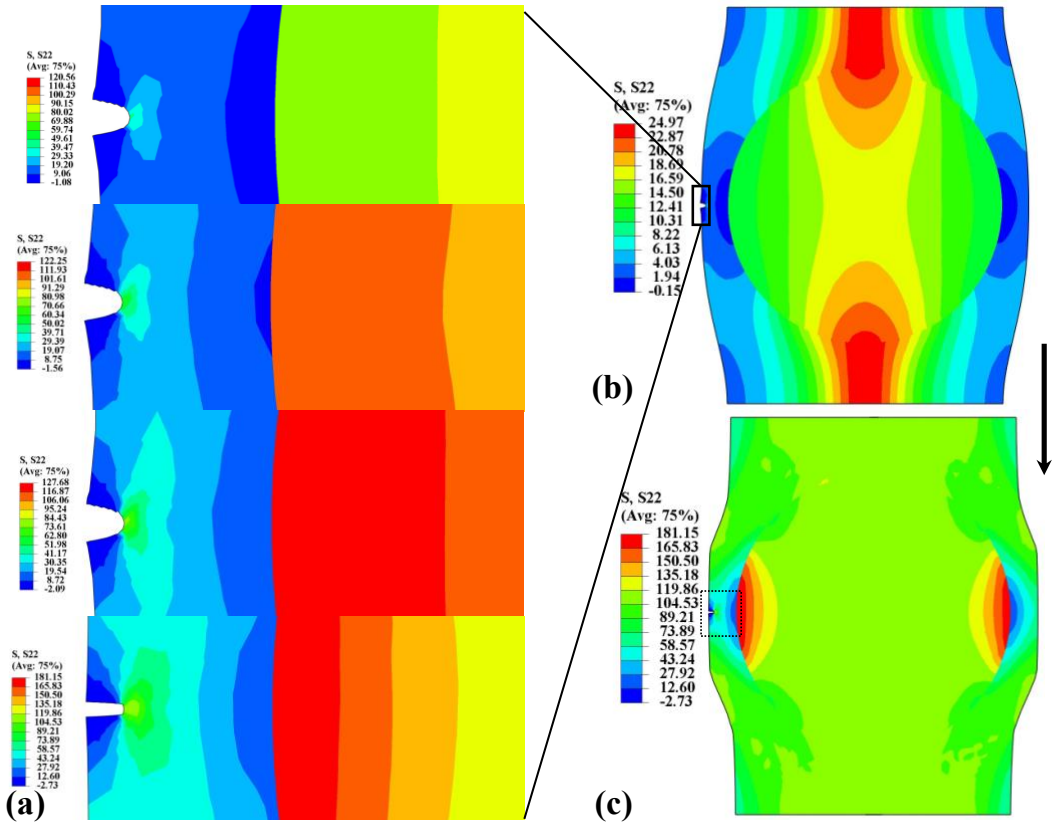

Fig. 4 The 2-directional stress distribution on the composites with deflection developing in time from (b) to (c), in which (a) shows a zoomed view for the propagation of the deflection.

From Figure 4(a), we can observe a local stress concentration at the end of the deflection. Such indicates that the high concentration of stress might elicit the local

failure of the matrix. For what is more, the evident local stress increasement can be observed compare Figure 4(c) with Figure 2(f). Generally, the stress σ_{22} did not significantly changed compared with the no deflection model presented in Figure 2. Notwithstanding, the local deflection increases the local, and thence, the total 2-directional stress.

Also, the total strain ε_{22} distribution with the matrix deflection is presented as in Figure 5, developing from (a) to (c). From such distribution one can observe that the local matrix deflection only slightly change the local strain at the beginning stage, albeit basically makes no variance on the strain in the following stages.

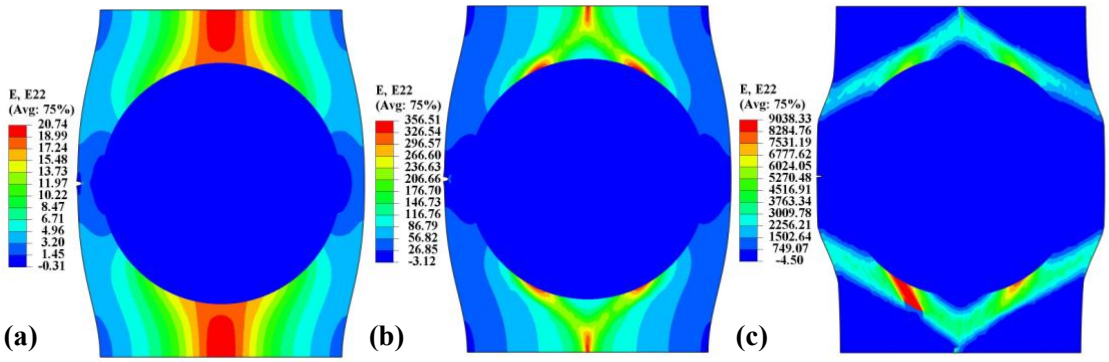

Fig. 5 The 2-directional strain distribution on the composites with deflection developing in time from (a) to (c).

The plastic strain distribution is shown in Figure 6 with the ongoing loading from (a) to (c), in which the deflection is taken into consideration.

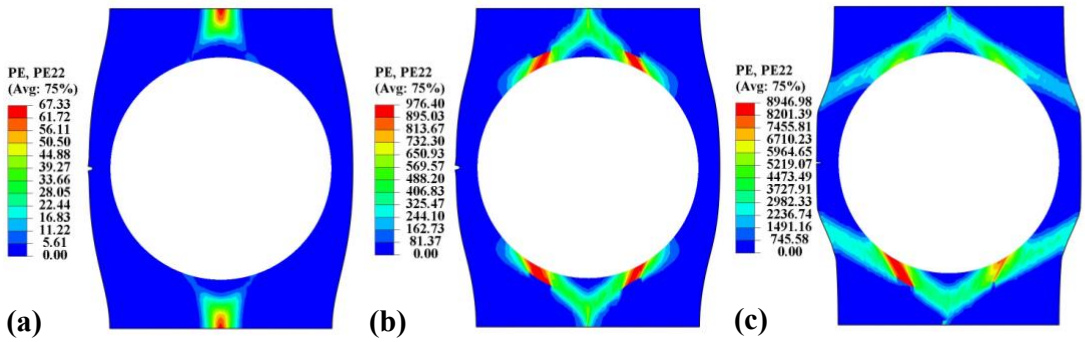

Fig. 6 The 2-directional plastic strain distribution on the composites with deflection developing in time from (a) to (c).

From Figure 6, one can discern that the matrix deflection makes no impact on the 2-directional plastic strain. Furthermore, the strain concentration along the central axis shown both in Figure 3(a) and Figure 5(a) is not plastic strain compared with Figure 6(a). the plastic strain grows from the loading edge to the tangential surface of fiber shown from Figure 6(a) to Figure 6(c).

Here, we also present a 2-directional stress-strain diagram of the matrix documenting the maximum value as shown in Figure 7.

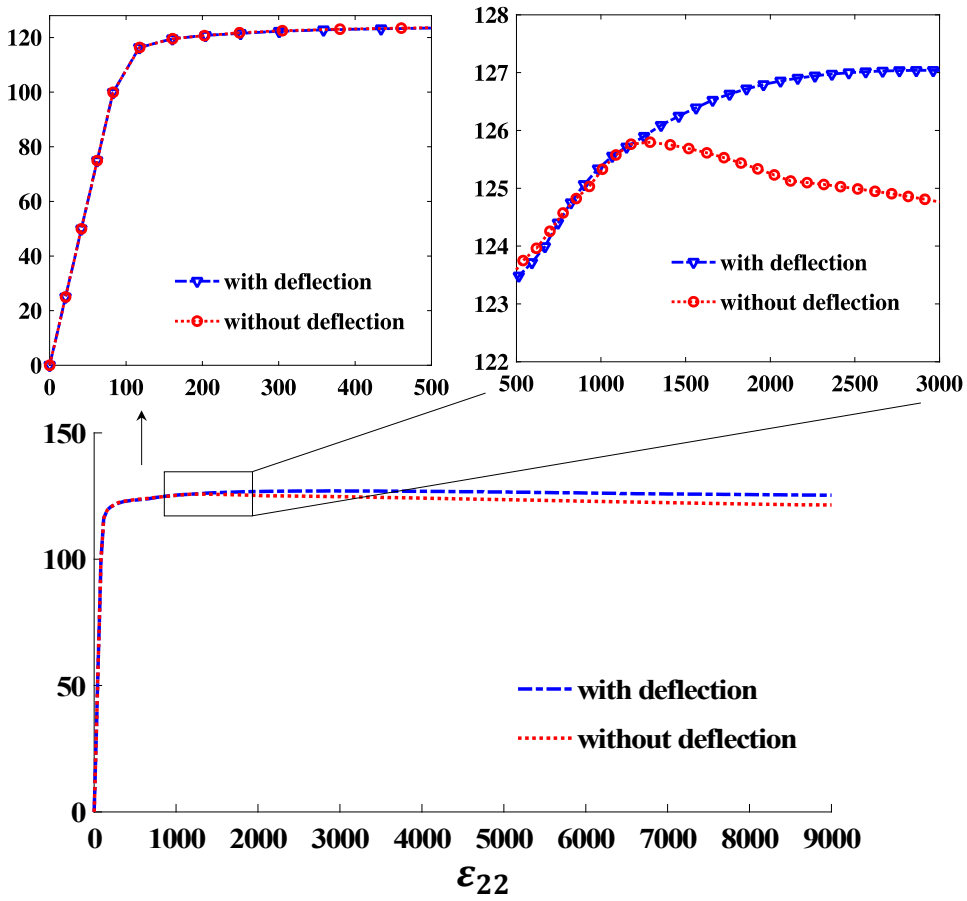

Fig. 7 The stress-strain curve of the composite with and without deflection, in which the unit is set to be [MPa].

From Figure 7, one can discern that the stress-strain curve coincides with each other at the beginning stage, including the elastic region and initial yielding state as shown in the left zoomed view. Notwithstanding, the yield region contends that the

model with a matrix deflection exhibits higher values of stress as shown in the right zoomed view, which can be illustrated and explained by Figure 4. Also, such impact indicates a higher possibility of the local fracture as discussed in the preceding paragraphs. For what is more, the right zoomed view also indicates how the stress fluctuated as the initial stress variation stage.

For both the simulation illustrations and the diagrams indicate the variation effect of the matrix deflection will increase the 2-directional stress, especially the area surrounding the deflection. Also, the plastic strain growth distribution indicates a possible failure mechanism of the fiber-reinforced composite, to fracture along the fiber's shearing surface.

Conclusion

The rate-independent stress update algorithm with the Drucker-Prager criterion is reasoned both from an analytical solution (Equation 1-Equation 23) and a numerical solution (Equation 24-Equation 35) and illustrated as in Box 1. The fiber-reinforced composite is estimated as a unit cell model through decent simulations carried out with a tensile loading as illustrated in Figure 1. The unit cell is discussed in which a comparison of the addition of the deflection. The material coefficients carried out for simulation are given in Table 1 and Table 2.

The simulation results show that with the no deflection model, the stress is centrally concentrated along the middle axis at the beginning stage (Figure 2(a)), and growing more evenly distributed on the composite yet robustly concentrated on the 2-

directional fiber edge (Figure 2(f)). A relatively low-stress value also occurs on the contact surface of the matrix (Figure 2(f)).

Also, the strain distribution shows that the strain displays similar trends with stress at the beginning stage, in which its value is highly concentrated along the central axis (Figure 3(a)), howbeit growing to highly concentrated along the shear surface of the fiber (Figure 3(f)).

When considering the existence of the local deflection on the matrix, the stress distribution generally follows the same as in without deflection (Figure 4(b), Figure 4(c)). Howbeit a local stress concentration occurs due to the deflection (Figure 4(a)). Specifically, the deflection elicits the stress concentration and the tail of the deflection. Also, the deflection model displays a similar strain distribution with the non-deflection model (Figure 3, Figure 5), only a small strain decrease at the deflection edge (Figure 5(a)). When discussing the plastic strain of the matrix, the deflection makes no difference in its distribution (Figure 6).

Of the stress-strain curve of the matrix (Figure 7), the deflection model displays higher stress value, which is explained and elucidated in the stress distribution (Figure 4). The curves coincide in the elastic region and the initial yielding stage (left zoomed view in Figure 7). Howbeit the stress fluctuates in a complex form at the beginning of yielding (right zoomed view in Figure 7).

Acknowledgement

The author would like to thank B. An for the valuable discussion.

References

[1] Jacob Lubliner [1990]. PLASTICITY THEORY.

[2] Alberto M Cuitiño. A material independent method for extending stress update algorithms tofinite plasticity with multiplicative kinematics. Engineering Computations. December 1992

[3] Ronaldo I. Borja. Plasticity, Modeling & Computation. DOI 10.1007/978-3-642-38547-6. 2013938490

[4] J.C. Simo and T.J.R. Hughes. Computational Inelasticity. 1998, Volume 7. ISBN : 978-0-387-97520-7

[5] D. Mohr. Integration Algorithms for Rate-independent Plasticity (1D). Lecture #4 – Fall 2015. ETH Zürich.

[6] Dynamic Behavior of Materials and Structures. Computer Lab #5, Page 4: Stress update algorithm on von Mises plasticity.

[7] H S Choi *et al* 2018 *J. Phys.: Conf. Ser.* **1063** 012011

[8] M. Rezania, N. Sivasithamparam, M. M. Nezhad. On the stress update algorithm of an advanced critical state elasto-plastic model and the effect of yield function equation. Finite Elements in Analysis and Design 90 (2014) 74–83

[9] B. An, H. D. Wagner. Role of microstructure on fracture of dentin. Journal of the Mechanical Behavior of Biomedical Materials. Vol 59 (2016): 527-537. ISSN 1751-6161.

[10] An B. Constitutive modeling the plastic deformation of bone-like materials. Int J of Solids Struct 2016; Vol 92–93: 1-8

[11] An B., Zhang D. Bioinspired toughening mechanism: lesson from dentin. Bioinspir. Biomim., 10 (2015), Article 046010

[12] B. An, D. Zhang. An analysis of crack growth in dentin at the microstructural scale. Journal of the Mechanical Behavior of Biomedical Materials 81 (2018) 149–160.

[13] B. An, Y. Xu, D. Zhang. Crack initiation and propagation in composite microstructure of dentin. International Journal of Solids and Structures 110–111 (2017) 36–43

[14] Xiong Zhang, Zhen Chen, Yan Liu. The Material Point Method, Academic Press, 2017, Pages 175-219, ISBN 9780124077164.

[15] M. Čermák, S. Sysala, J. Valdmane (2018). Efficient and flexible MATLAB implementation of 2D and 3D elastoplastic problems. Applied Mathematics and Computation.

[16] M. Čermák, S. Sysala, and J. Valdman. Matlab FEM package for elastoplasticity. 2018.

[17] H. Teng. Effective elastic–plastic response of two-phase composite materials of aligned spheroids under uniaxial loading. Mechanics of Materials 117 (2018) 91–104.

[18] A. Behnam, M. D. Denavit. Plastic stress distribution method for predicting interaction strength of steel-concrete composite cross sections. Journal of Constructional Steel Research 170 (2020) 106092.

[19] M. Majewski, P. Holobut, M. Kursa, K. Kowalczyk-Gajewska. Packing and size effects in elastic-plastic particulate composites: Micromechanical modelling and numerical verification. International Journal of Engineering Science 151 (2020) 103271

[20] C. He, J. Ge, B. Zhang, J. Gao, S. Zhong, W. K. Liu, D. Fang. A hierarchical multiscale model for the elastic-plastic damage behavior of 3D braided composites at high temperature. Composites Science and Technology 196 (2020) 108230

[21] M. Zscheyge, R. Boehm, A. Hornig, J. Gerritzen, M. Gude. Rate dependent non-linear mechanical behaviour of continuous fibre-reinforced thermoplastic composites – experimental characterisation and viscoelastic-plastic damage modelling. Materials & Design.